



Application of hyperspectral imaging for characterization of VOC-induced historical glass corrosion

Deepshikha Sharma^{1,3,a} , Katharina Schmidt-Ott^{1,b}, Ulrike Rothenhäusler^{1,c}, Sony George^{2,d}, Edith Joseph^{3,4,e}, Tiziana Lombardo^{1,f}

¹ Collection Centre, Swiss National Museum, Lindenmoosstrasse 1, 8910 Affoltern am Albis, Zurich, Switzerland

² Department of Computer Science, Norwegian University of Science and Technology, Teknologivegen, 2815 Gjøvik, Innlandet, Norway

³ Laboratory of Technologies for Heritage Materials, University of Neuchâtel, Av. de Bellevaux 51, 2000 Neuchâtel, Switzerland

⁴ Haute Ecole Arc Conservation Restauration, University of Applied Sciences and Arts Western Switzerland HES-SO, Espace de l'Europe 11, 2000 Neuchâtel, Switzerland

Received: 6 November 2022 / Accepted: 15 February 2024

© The Author(s) 2024

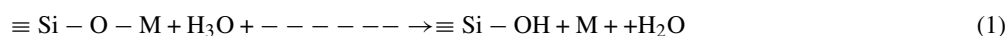
Abstract Hyperspectral imaging (HSI) provides high-resolution recording of the spectral information at every spatial point (pixel) of an object throughout a contiguous range of wavelengths. This paper reports an attempt at exploring the application of HSI in transmittance mode for the identification and quantification of corrosion in transparent historical glass, which is difficult to identify by visual inspection. This was done using model glass samples mimicking historical composition and subjected to artificial ageing in the presence of volatile organic compounds. Hyperspectral images of unaged and aged glass samples were recorded with two cameras covering visible and near infrared (VNIR, 400–1000 nm) and short-wave infrared range (SWIR, 1000–2500 nm) using a custom-made HSI set-up in transmission mode. The HSI data were further processed to classify and visualize corrosion in different ageing environments and ageing periods. The results show that HSI can be employed as a valuable tool to assess glass corrosion at early stages, especially by analysing the SWIR spectral region—which shows the water absorption by the glass matrix due to corrosion.

1 Introduction

Within the Cultural Heritage Analyses for New Generations (CHANGE) project framework (www.change-itn.eu), this research focuses on various degradation phenomena that were detected on historical glass objects belonging to seventeenth–twentieth century stored in mobile chipwood shelving units for about 32 years in uncontrolled temperature and relative humidity (RH) in the old depot of the Swiss National Museum (SNM) [1].

Chipwood is well known to emit volatile organic compounds (VOC) [2, 3], mainly formaldehyde, formic acid and acetic acid [4] which could exacerbate the corrosion process in historical silicate glass objects kept in museums [5–7]. Degradation phenomena such as cracking and salt neocrystallizations were visually detected on historical objects in the museum collection [1]. Chemical analyses of three of the most severely corroded historical glass objects were carried out using Fourier transform infrared spectroscopy, and the presence of formates and acetates on the surface was ascertained [8]. The objects were found to be potash–lime–silicate glasses using scanning electron microscopy coupled with electron-dispersive X-ray spectroscopy (SEM–EDX) [9].

Analysing and imaging corroded glass is a challenging task. The main objective of this research project is to establish a methodology and protocol based on non-destructive imaging techniques to identify VOC-induced glass corrosion in historical objects. Depending on the atmospheric conditions, glass corrosion starts with the formation of a water film on the surface, allowing ionic exchange between the H^3O^+ ions of water and the ions (main alkaline elements such as K and Na, and in a lesser extent earth-alkaline elements such as Ca) present in glass. This phenomenon leads overtime to the physisorption of molecular water into the glass matrix (hydration) and to the formation of a layer rich in silica and depleted in alkali (leaching) according to the equations below:



^a e-mail: deepshikha.arch@gmail.com (corresponding author)

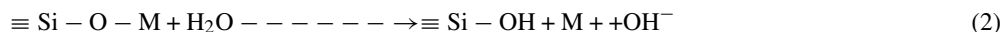
^b e-mail: Katharina.Schmidt-Ott@nationalmuseum.ch

^c e-mail: Ulrike.Rothenhaeusler@nationalmuseum.ch

^d e-mail: sony.george@ntnu.no

^e e-mail: Edith.Joseph@he-arc.ch

^f e-mail: Tiziana.Lombardo@nationalmuseum.ch



with M an alkaline element: K, Na or an alkaline-earth element: Ca...

The leached alkali (or earth-alkali) can react with anions present in the environment and form corrosion products on the glass surface in the form of wet or dry salt neocrystallizations [10–12]. The leaching reaction often promotes the accumulation of a strongly alkaline hydroxyl solution (2). In a second phase, as the surface pH increases, network dissolution due to hydrolysis starts when hydroxyl OH^- ions present in water break the Si–O–Si bonds (3).



Therefore, the changes in H_3O^+ and OH^- ions present in glass could be useful for characterizing corrosion. Rice et al. [13] shows that short-wave infrared range (SWIR) could provide various information about water molecules present in silica, which can also be detected in silicate glass matrix because of water uptake during corrosion. The most important bands are ≈ 1410 nm showing OH^- overtone, ≈ 1470 nm showing H_2O overtone or combination, ≈ 1910 nm indicating H_2O molecules in silica cages (almost free from hydrogen bonding) and ≈ 1940 – 1960 nm indicating hydrogen-bonded H_2O molecules in voids or films on silica surfaces. Indeed, the prominent bands around ≈ 1415 nm and ≈ 1905 nm were successfully used by Zaleski et al. [14] and Brostoff et al. [15] for the characterization of glass corrosion using fibre optic reflectance spectroscopy (FORS). However, FORS provides single point measurements without comprehensive spatial information.

Hyperspectral imaging is a technique based on the high-resolution recording of spectral reflectance at every spatial point (pixel) of the object throughout a contiguous range of wavelengths within the electromagnetic spectrum [16]. This technique records both spectral and spatial data for an object at the same time and therefore has been applied to several research areas. Throughout a specific spectral range, spectral reflectance (i.e. reflectance per unit of wavelength) can be transformed into a spectral reflectance curve and it depends on various factors such as the illumination, the viewing geometry, the detector sensitivity as well as the material properties of the object being examined [17]. Originally developed for geological and mineralogical research and remote sensing [18], HSI is relatively new in the field of cultural heritage and has already given promising results on historical artworks and documents [17, 19, 20] and references therein. Physical (e.g. colour) as well as chemical information (composition) of the material being analysed can be obtained by the detection of the vibrational absorption bands observed at different wavelengths on their reflectance spectrum. The visualization of the distribution of specific compounds is also possible.

Glass, as a material, has not been extensively investigated by HSI. Studies by [21–25] showed the use of HSI to identify the chromophores in stained glass using visible and near-infrared range (VNIR). A recent work was done on glass fibre composites to map their degradation due to thermal loading using HSI [26]. A patent, by Hong Jin Gwang, for an HSI system to detect defects on mobile cover glass, bare glass and film was published in 2016 [27]. These are the closest to any approach towards detecting degradation signs on transparent glass using HSI. Nonetheless, there is no other reported work on characterization of glass corrosion using HSI. Therefore, it is important to ascertain the potential of hyperspectral imaging (HSI) for the assessment and monitoring of historical glass objects that are undergoing continuous degradation. This will be explored in the present paper.

2 Methods

To establish the required protocol for historical objects, the methodology is being developed on model glasses, which are artificially corroded. These allow for the study of early stages of corrosion and provide logistical ease to travel for analyses.

The model glasses are prepared by traditional glass blowing technique to replicate the high-potassium–lime–silicate composition of three of the most corroded historical glass objects from the collection of the SNM (model glass composition given in supplementary material). The model glasses are first blown into cylinders and then sectioned into curved rectangular pieces of roughly 5×3 cm size and 1–2 mm thickness [9]. They are engraved with three lines each on the two long sides, to mimic the decoration of the historical objects and labelled individually (Fig. 1a). They were placed vertically on glass stands inside the ageing set-up.

Three different conditions are selected for the artificial ageing of the model glasses using borosilicate glass desiccators in ambient temperature of 20–25 °C and RH controlled using preconditioned silica gel.

1. High VOC concentration (acetic acid $\approx 3000 \times 10^3 \mu\text{g}/\text{m}^3$ + formic acid $\approx 1250 \times 10^3 \mu\text{g}/\text{m}^3$) and alternating RH (PV).
2. Low VOC concentration (acetic acid $\approx 6000 \mu\text{g}/\text{m}^3$ + formic acid $\approx 5000 \mu\text{g}/\text{m}^3$) and alternating RH (V).
3. High VOC concentration and fixed humidity at 50% (P).

The RH cycles were alternating at 35 and 70% (PV and V) for 17 months, resulting in an equal number of days at 35 and 70% RH.

The VOC concentrations were measured during the ageing using photo-ionic detector as well as passive samplers. However, the reliability for both of them could not be established.

For each of the above three conditions, one batch of eight model glass samples is withdrawn and characterized at an interval of 3–5 months, up to a period of 17 months. In total, five batches of eight samples are withdrawn from each of the three ageing conditions. One batch of ten samples is kept as reference at 20–25 °C and 45–50% RH.

Fig. 1 RGB photographs of PV glass in transmitted light **a** before ageing, **b** after 12 months ageing

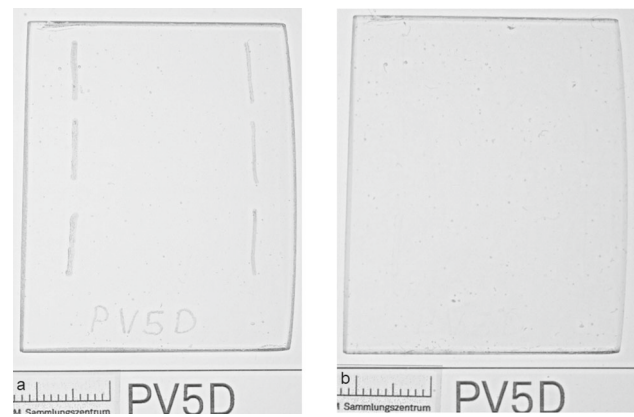
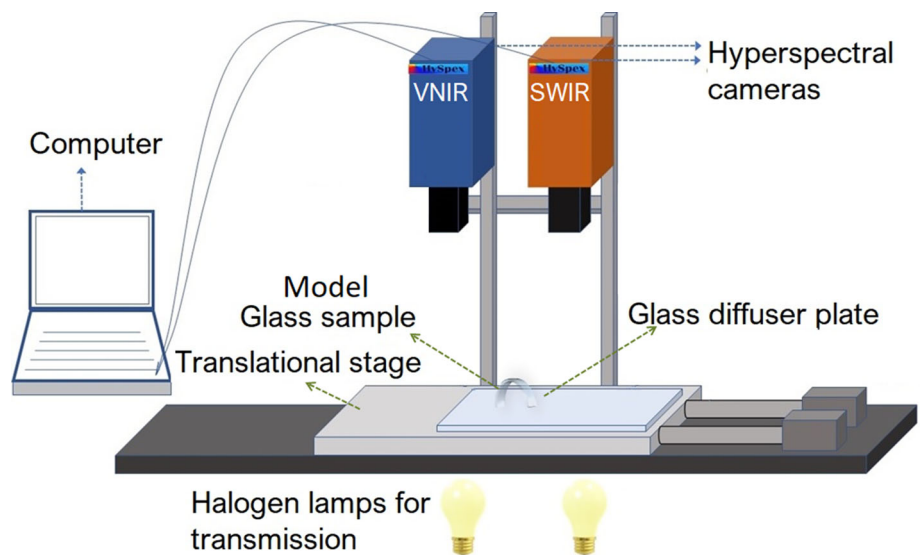


Fig. 2 Schematic diagram of the HSI set-up in transmission mode using both VNIR and SWIR cameras



2.1 Hyperspectral imaging (HSI)

Hyperspectral image acquisition is carried out using two imaging systems: a HySpex VNIR-1800 and a SWIR-384 push-broom system, both developed by Norsk Elektro Optikk As. The VNIR camera takes 186 images each of 1800 pixels in a single line. Every image corresponds to a spectral sampling of 3.26 nm between 400 and 1000 nm. Similarly, the SWIR camera takes 288 images each of 384 pixels in a single line and each image corresponds to a spectral sampling of 5.45 nm between 1000 and 2500 nm. Experiments are conducted at Colourlab, NTNU Norway.

Trials are performed with different light sources and geometric positions, imaging parameters and reflected or transmitted light, to identify the best configuration for the acquisition of the corroded model glass samples. Tests are performed to check the influence of the sample curvature in the obtained data transmittance measurements and clearly show no noticeable modifications when compared to a flat surface. Eventually, the optimal configuration is defined as followed. The HSI data are collected in transmittance mode (Fig. 2). Halogen lamps are used as the light sources and are placed below a moving translation stage in a way that radiation from one light source will be transmitted through a glass diffuser plate with enough intensity to reach the camera through the model glass sample to be studied. The camera focuses on the top of the glass sample, and images are acquired with two lenses of focal distance 3 and 30 cm (distance between the camera and the object) in both VNIR and SWIR. Acquisition parameters such as integration time and frame averaging are set and are synchronized with the speed of the moving stage controlled using a computer software provided by the camera manufacturer. All the image acquisitions are performed in a dark room to avoid any stray light recorded in the sensor.

The acquisition time for a whole model glass sample is approximately two minutes, and the heat at the sample surface generated by the halogen lamps is constantly monitored using a thermal camera during acquisition. This way it is ensured that the temperature during light exposure was ≈ 30 °C, which is considered to be safe for the model glass (and eventually for the historical glass objects) [28].

Data from ten unaged reference model glass samples along with two model glass samples from each of the ageing condition and ageing periods are presented in this paper. The raw data initially need to be corrected to radiance using HySpex-RAD software provided by the camera manufacturer. The software automatically corrects for factors like quantum efficiency of the sensor, dark

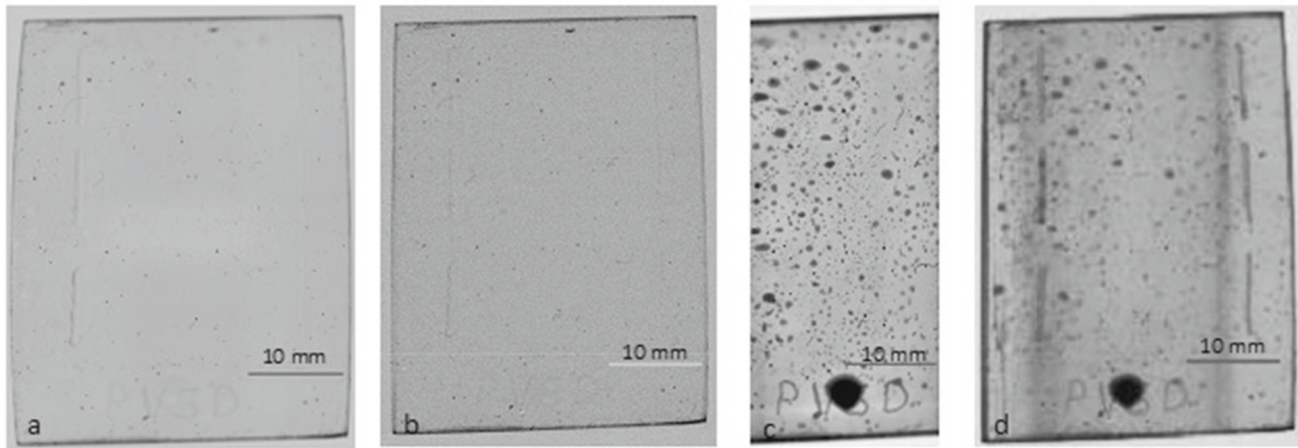


Fig. 3 Hyperspectral image of PV model glass sample aged for 12 months at 700 nm (VNIR) with **a** 3 cm and **b** 30 cm lens and at 1906 nm (SWIR) with **c** 3 cm and **d** 30 cm lens

current, etc., which are not influenced by the sample shape. Sensor corrections are automatically done by the software. The study focuses on specific spatial points that are not influenced by the overall global geometry of the sample. After the radiance correction, the acquired data cubes are transformed into transmittance, by dividing each of them by an image of the diffuser alone, with the same size of the image and illumination condition as that of the sample. Since dark current subtraction is already done by the software, transmittance then is calculated by the formula (4).

$$T = \frac{S_{x,\lambda}}{W_{x,\lambda}} \quad (4)$$

where $S_{x,\lambda}$ is the light signal transmitted by the object and $W_{x,\lambda}$ is the light signal transmitted by the diffuser alone, at pixel location x, λ . Indices x, λ indicate, respectively, pixels across the track and the number of bands (1800 and 186 for VNIR; 384 and 288 for SWIR, respectively) [24].

HSI images were processed for spatial and spectral data using open-source Fiji distribution of ImageJ software [29]. Spectragryph [30] was used to calculate the integral (area under the peak) of the significant vibrational bands identified in the spectra collected.

2.2 Transmittance spectroscopy (TS)

In order to validate the acquired HSI data, TS on selected model glass is performed. PV model glass aged for 3, 6, 9 and 12 months along with one reference (unaged model glass) is measured using the LAMBDA 1050 UV/Vis/NIR spectrophotometer from PerkinElmer, which is a double beam, double monochromator, ratio recording UV/Vis/NIR spectrophotometer (250–2500 nm) with a wavelength accuracy of ± 0.080 nm in UV/VIS range and ± 0.300 nm in the NIR range. The data are treated to remove a noisy region beyond 2100 nm.

3 Results

3.1 Data selection

Hyperspectral images acquired at a distance of 30 cm from the camera to the glass offered a good visualization of the whole sample in both SWIR and VNIR range (Fig. 3b and d) while offering enough depth of field to visualize both the faces of the model glass without any blurring. While the HSI acquired at a closer distance (3 cm) could only document part of the model glass in SWIR ($\approx 5 \times 2$ cm) and the whole sample in VNIR (Fig. 3a and c). The 3 cm lens however gives a better-resolved image with more clarity in comparison with the more pixelated image from 30 cm lens, especially for visualizing cracks.

On the spectral processing side, the quantification of the corrosion extent is retrieved from the data obtained with the 30 cm lens from the whole model glass for SWIR and for VNIR both.

3.2 Spectral information from VNIR and SWIR

The VNIR spectra of unaged and aged model glass in the three different environments (P, PV and V) are found to lack any special features between 400 and 1000 nm (Fig. 4) in accordance with existing literature [31]. In addition to this, since the curves obtained for both unaged and aged model glass are very similar, it is concluded that the spectral information in VNIR is not relevant to identify

Fig. 4 VNIR average spectra of glass samples from P (blue), PV (purple) and V (yellow) condition aged for 12 months compared with unaged reference glass (Ref, grey)

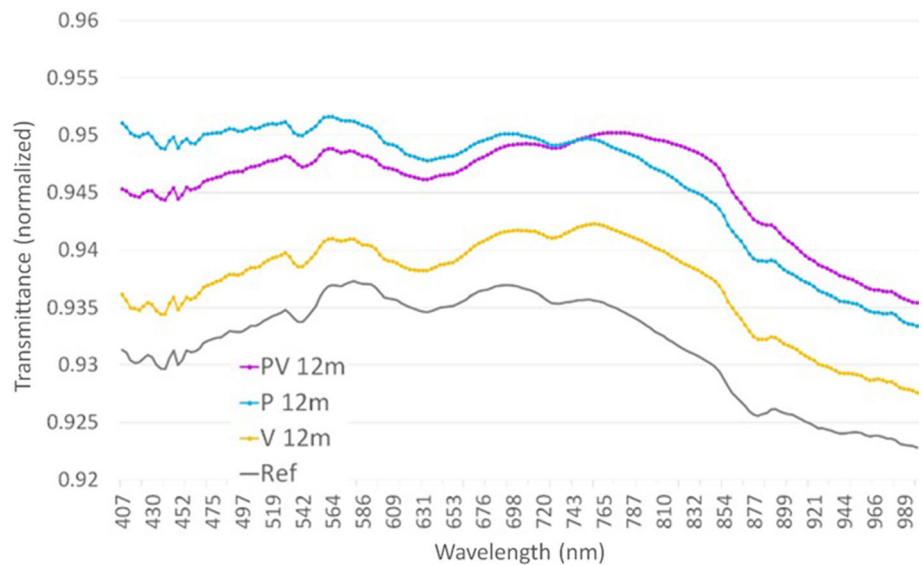
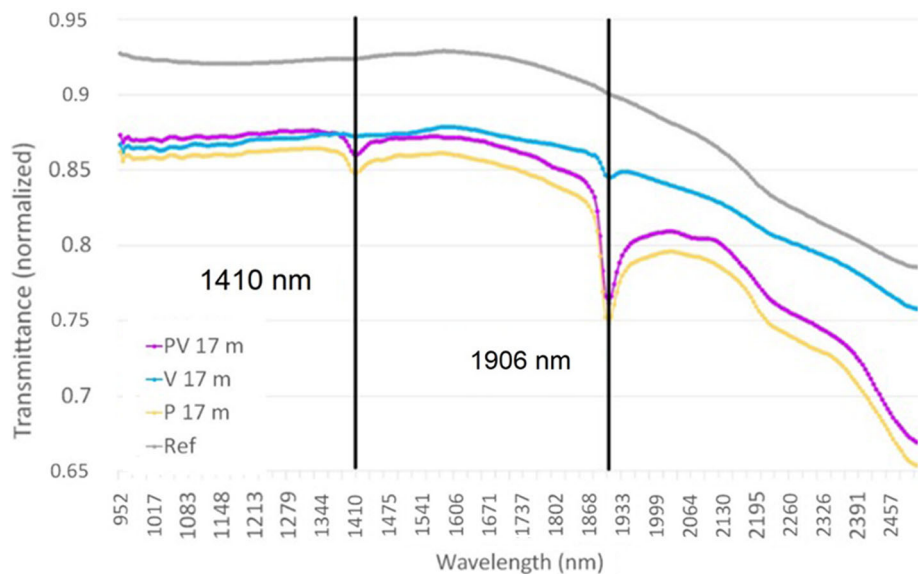


Fig. 5 SWIR average spectra of PV (purple), P (yellow) and V (blue) model glass samples aged for 17 months along with the reference spectra (Ref, grey)



corrosion. Nonetheless, VNIR images show features, also visible, with naked eyes such as cracks, engravings, label, bubbles and dust particles at a high spatial resolution (Fig. 3a and b).

The SWIR average spectra for the model glass samples in the P and PV conditions aged for 17 months show two prominent peaks ≈ 1410 and ≈ 1906 nm, which do not occur in the unaged reference glass (Fig. 5). These indicate the presence of OH^- species and molecular water absorbed in the corroded model glass matrix, respectively. The spectrum of V glass, however, does not show the peak at ≈ 1410 nm similar to unaged reference but only at ≈ 1906 nm. Finally, the ≈ 1906 nm peak intensity shows significant differences between samples aged in P and PV versus V condition.

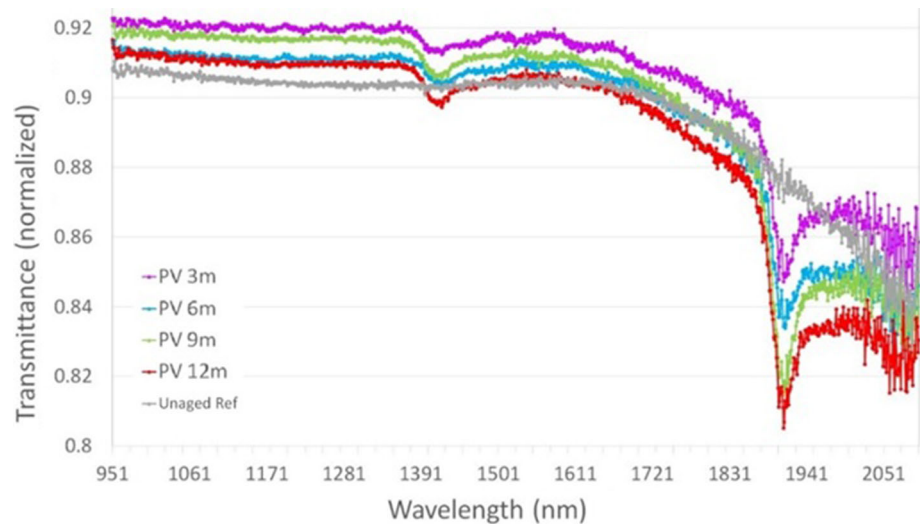
TS is also performed on PV model glass samples on random points. Results show the peaks at ≈ 1410 and ≈ 1906 nm for the glass samples aged in PV condition validating the HSI results (Fig. 6).

3.3 Data visualization: spatial distribution of corrosion in glass

The grey value (transmittance) distribution across a rectangular area taken at the bottom of the sample (Fig. 7a and b; white rectangle in Fig. 7c) shows four distinct regions (Fig. 7d) of corrosion on the model glass sample. Lower the grey values, lower is the transmittance and accordingly the pixel appears darker.

The different grey levels (indicating the transmittance at this distance inside the white rectangle in Fig. 7c) discernible in this image allow the identification of four main regions; for each of these, a representative spectrum extracted at point 1–4 is also shown in Fig. 7e:

Fig. 6 TS spectra of PV model glass aged for 3 (purple), 6 (blue), 9 (green) and 12 (red) months along with the unaged reference (unaged Ref, grey)



1. Light grey region vertically on left and right side of the sample centre (demarcated by blue colour in Fig. 7d and with 1 in Fig. 7c). The spectrum shows peaks at ≈ 1410 and ≈ 1906 nm, indicating the presence of molecular water and OH^- species, respectively.
2. A darker grey region mostly in the sample centre (demarcated by yellow colour in Fig. 7d and with 2 in Fig. 7c). A representative spectrum of this area (taken at point 2) shows peaks at ≈ 1410 and at ≈ 1906 nm; the intensity of the latter peak is higher than that at point 1.
3. A pair of dark grey lines running vertically on left and right side of the sample (demarcated by green colour in Fig. 7d and with 3 in Fig. 7c). The spectrum shows peak at ≈ 1410 and ≈ 1906 nm. The intensity at ≈ 1906 nm is higher than that at point 1 and 2. This indicates a higher extent of molecular water absorption. All these features are not visible with naked eyes or with RGB photography in transmitted light (Fig. 1b).
4. Dark black circular spots (demarcated by red colour in Fig. 7d and with 4 in Fig. 7c) are characterised by very broad and intense bands between ≈ 1410 – 1470 nm (OH^- and H_2O overtones) and ≈ 1906 – 1960 nm (water molecules inside silica cages and as films on the surface). Indeed, these are wet salt neocrystallizations of deliquescent formate salts (chemically assessed by Raman spectroscopy and imaged using digital microscopy). These are also visible with naked eyes but cannot be seen with RGB photography in transmitted light (Fig. 1b).

Thus, the visualization as well as the spectra clearly shows non-homogeneous water uptake by the glass matrix during corrosion. Additionally, no cracks were observed on the concave face of the P and PV model glass as well as on V model glass.

3.4 Temporal evolution of corrosion and comparison of ageing environment

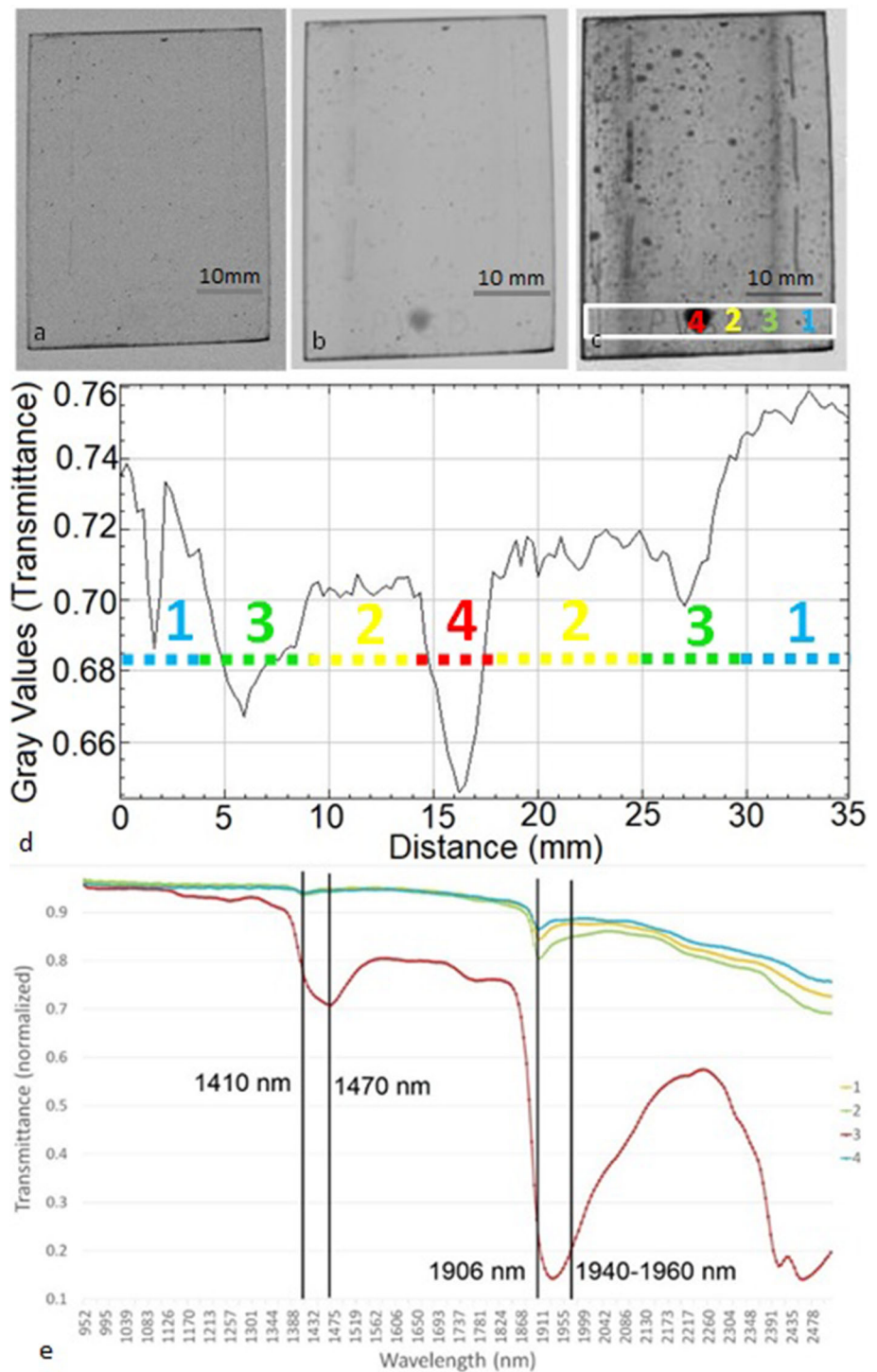
In order to understand the temporal progression of corrosion, SWIR images and spectra of model glass samples withdrawn at different ageing periods were compared (Figs. 8 and 9).

For PV and P samples, the four distinct regions already described in the previous section can be seen starting from 3 months of ageing (Fig. 8). Variations in the size and position of the different features can be visualized over the course of the ageing progression. Additionally, certain features especially the dark lines (region 3) become even darker after 12 and 17 months ageing (Fig. 8d, e, j, k). Although these lines are not visible with naked eyes (or VNIR-HSI imaging), it is important to note that the 17-month-aged P and PV samples show preferential visible cracking along these lines (Fig. 8e–f and k–l). V samples do not show such distinct regions and dark lines until 12 months (Fig. 8m–p). At 17 months, a pair of faintly dark lines at the centre of the sample (Fig. 8q) can be seen. These dark lines are interpreted to be due to some surface discontinuities developed on the model glass surface as a result of manufacturing which are preferentially corroded by the surface run-off of large wet salt neocrystallizations across the length of the model glass samples due to gravity, since the samples were kept in vertical position inside the desiccators during the ageing. Such wet salt neocrystallizations can be formed due to the repeated coalescence of small salt neocrystallizations. The dark circular features are verified to be wet salt neocrystallizations using digital microscopy (DM) images as well (example shown in Fig. 9a and b) (analytical parameters given in supplementary material).

The heterogenous distribution of the corrosion with time can also be investigated using the spectral information. The average spectrum of two PV samples from each ageing period shows a progressive peak intensity increase at ≈ 1410 and to a higher extent at ≈ 1906 nm (Fig. 10).

The peak at 1906 nm was also used to understand the differences between the extents of corrosion in the different periods and conditions. For every SWIR spectrum, the integral of the area between 1876 and 1936 nm ($I_{1876-1936}$) is calculated in reference to its

Fig. 7 PV model glass sample aged for 12 months: VNIR image at **a** 700 nm; SWIR image at **b** 1410 nm **c** 1906 nm representing four visually distinct regions of corrosion **d** grey values (indicating transmittance at this distance) of area in white rectangle demarcating the four visually distinct regions **e** SWIR spectra corresponding to point 1 (blue), 2 (yellow), 3 (green) and 4 (red)



individual baseline and plotted in Fig. 11. $I_{1876-1936}$ linearly increases with ageing period for both P and PV conditions while there is no such clear trend for V. Moreover, it is slightly higher for condition P as compared to PV for every ageing period. However, observing the maximum and minimum values for both of them, there is not a significant difference in the extent of corrosion between P and PV. Therefore, this suggests that the concentration of VOC has a significant effect on the corrosion rate. In fact, V samples were aged at much lower VOC concentration as compared to P and PV samples. The role of alternating humidity (PV) versus fixed humidity (P) could not be established with the number of samples analysed with HSI.

The $I_{1876-1936}$ are also compared with the thickness of the alteration layer (AL) obtained by SEM imaging (analytical parameters given in supplementary material) (Table 1) for P and V model glass. AL thickness shows an increasing trend for P model glass,

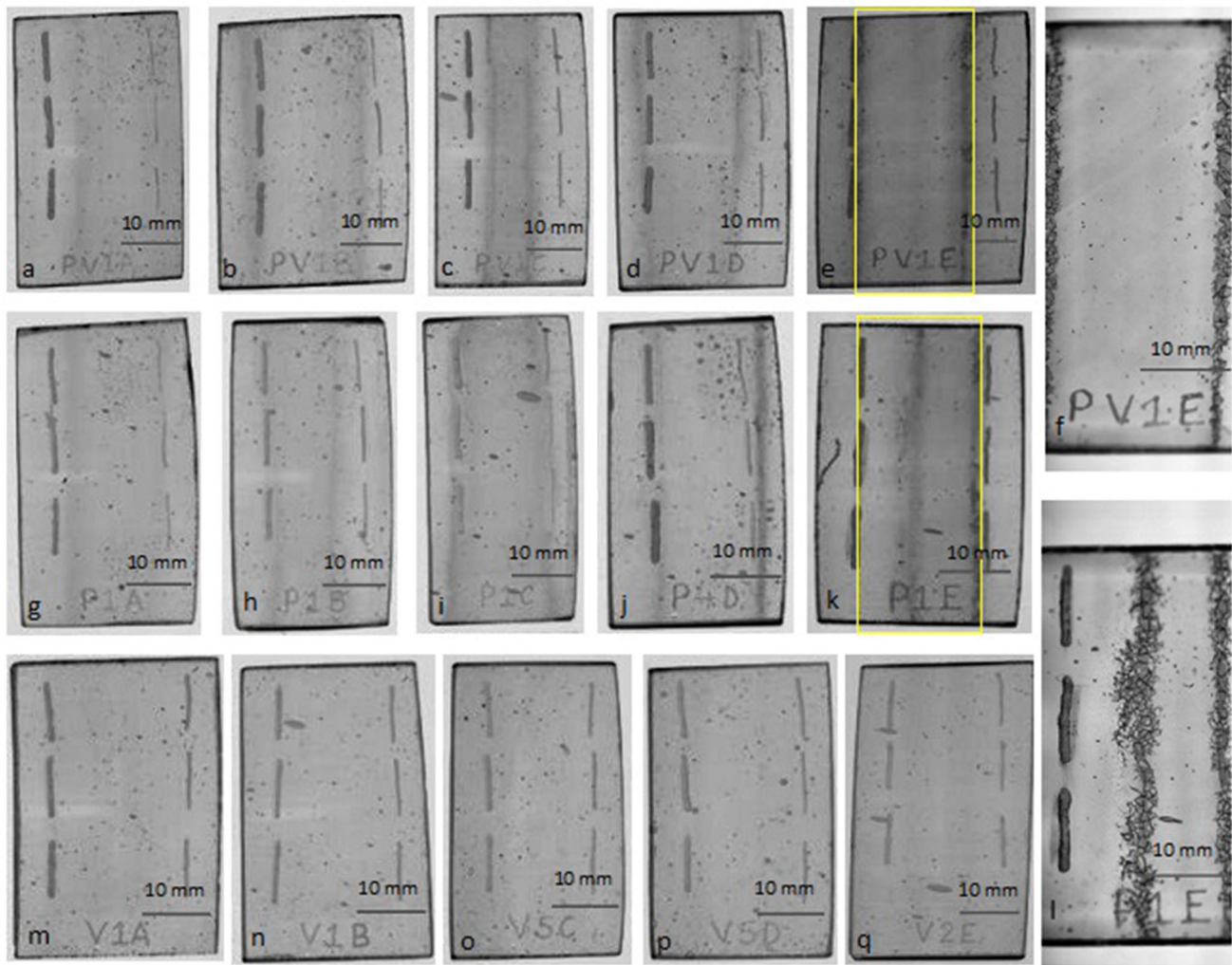
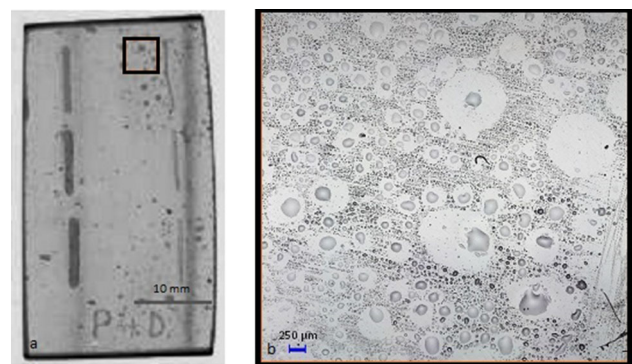


Fig. 8 SWIR images recorded with 30 cm lens (1906 nm) of PV model glass sample aged for **a** 3, **b** 6, **c** 9, **d** 12 and **e** 17 months, **f** 17 months recorded with 3 cm lens; P model glass sample aged for **g** 3, **h** 6, **i** 9, **j** 12 and **k** 17 months, **l** 17 months recorded with 3 cm lens; V model glass sample aged for **m** 3, **n** 6, **o** 9, **p** 12 and **q** 17 months

Fig. 9 **a** SWIR image of P model glass aged for 12 months at 1906 nm indicating area selected for digital microscopy by black rectangle, **b** digital microscopy image of the area inside black rectangle on P model glass aged for 12 months at 100 × original magnification



and the values are much higher than those of V model glass. As expected, there is a large variation in the thickness across the samples given the highly heterogeneous nature of glass corrosion and the localized nature of SEM-EDX analyses. In case of P model glass, the AL thickness is 5.24 μm after 3 months of ageing which increases up to 13 μm by 6 months and further does not show increase until after 17 months of ageing. In case of V model glass, only 9- and 17-month-aged samples are analysed showing similar AL thickness of approximately 3 μm . It can be concluded thus that SWIR data showing a linear increasing trend for P are more representative due to its global scale acquisition as compared to the SEM-EDX results. With the present results it can be seen that SWIR imaging is able to detect an alteration layer of as low as about 3 μm .

Fig. 10 SWIR average spectra of PV model glass aged for 3 (purple), 6 (cyan), 9 (green), 12 (red) and 17 (yellow) months (m) along with reference glass (Ref, grey)

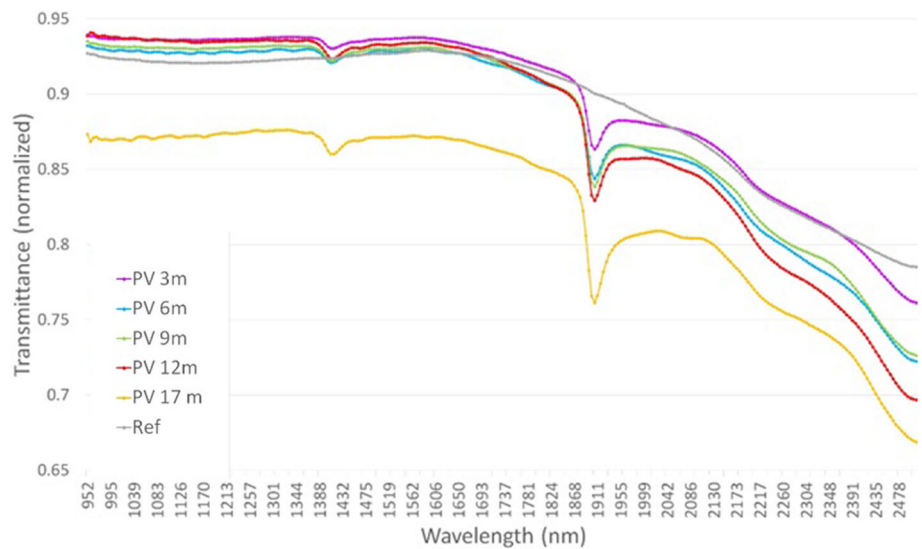


Fig. 11 Temporal progression of the average of the integral area between 1876 and 1936 nm for P (blue), PV (orange) and V (grey) conditions

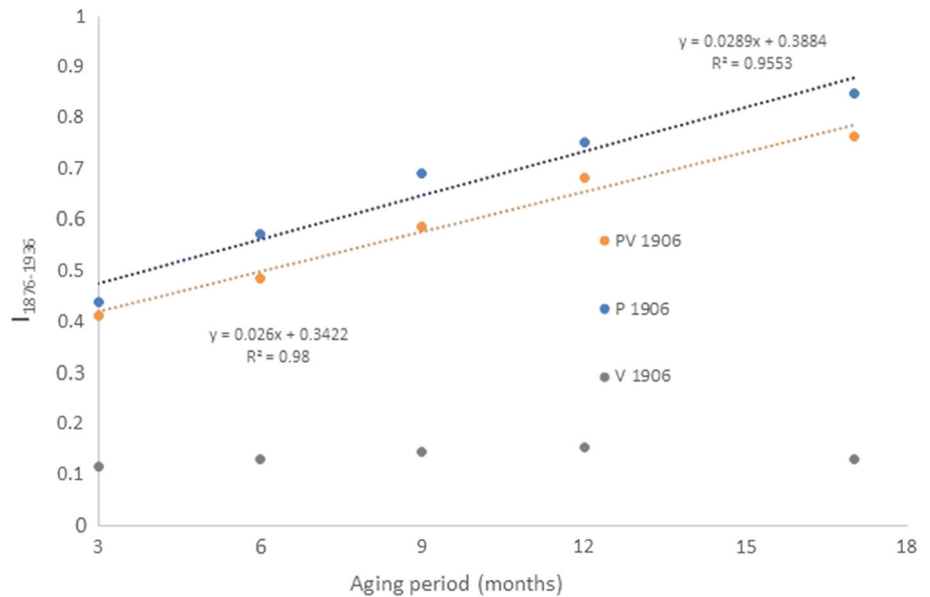


Table 1 $I_{1876-1836}$ values compared with average thickness of the alteration layer measured by SEM-EDX along with standard deviation for P and V model glass

V model glass	3 months	3 months	3 months	3 months	3 months
P- $I_{1876-1836}$	0.44	0.57	0.69	0.75	0.85
P-SEM-EDX AL thickness	5.24 ± 2.31	13.28 ± 0.17	12.81 ± 6.36	13.01 ± 0.28	16.24 ± 10.28
V- $I_{1876-1836}$	0.12	0.13	0.14	0.15	0.13
V-SEM-EDX AL thickness	–	–	3.1 ± 0.47	–	3.20 ± 0.57

Due to logistical constraints, it was decided that only the convex face of the samples will be analysed to measure the alteration thickness by SEM-EDX. Since the samples were vertically standing in the desiccator, both faces must be altered and contributing to the HSI imaging data, but this could not be measured. Assuming that both the faces were similarly corroded, the AL thickness measured could be doubled. Therefore, with the present results it can be seen that SWIR imaging is able to detect an alteration layer of as low as approx. $6 \mu\text{m}$.

4 Conclusions

HSI in the SWIR range is a non-invasive and non-destructive technique, which is proved to be successful in visual and chemical characterization of corrosion in the aged model glass samples, especially with the ≈ 1906 nm peak, which shows the extent of the hydration as well the heterogeneous distribution of water uptake by the glass matrix. Glass samples at high VOC concentration show vertical lines developed due to surface run-off of wet salt neocrystallizations across surface discontinuities created during manufacturing. Clearly these lines displayed higher extent of corrosion than the rest of the sample. With time, these lines indicated preferential zones for cracking development, as seen in samples aged for 17 months. Furthermore, the integral of the band centred at 1906 nm ($I_{1876-1936}$) can be used to obtain an estimation and therefore compare the extent of hydration between different ageing environments and periods. The ≈ 1410 nm peak seems to correspond to advanced stages of corrosion since it indicates changes in the OH^- species indicating leaching and possible network dissolution due to hydrolysis.

Results showed that P and PV samples corroded in high VOC concentration show much greater extent of corrosion compared with V samples corroded in low VOC concentration. Nonetheless, the influence of fixed versus alternating humidity is not established yet. Fortunately, V corresponds closest to the actual conditions for historical glass objects in the chipwood mobile shelving units of the old depot of the SNM and in general to what is found in indoor environments.

The application of HSI can provide information, which cannot be discerned by naked eyes, specifically the dark lines across the corroded model glass samples, which seem to be the precursors of cracks. In case of V with lower corrosion extent the visualization of any change with the photos was ineffective, so the contribution of the concave face would not make any difference. Probably, for P and PV with higher corrosion extent this could have some contribution which was not taken into account. In comparison with TS, which is a point measurement, HSI gives global level spatial and spectral data within a much shorter acquisition time and will be further explored on actual 3D historical glass objects. A combination of SWIR images at different wavelengths along with visual inspection could lead to proper monitoring of glass corrosion. A further comparison with SEM–EDX results of alteration layer thickness was attempted. However, the correlation between the HSI measurements and the alteration layer thickness is not straightforward since the former accounts for alteration on both the faces while the latter was measured only for the convex face. Assuming that the concave face must also be altered in all of the samples similar to the convex face, calculating a correlation is possible by assuming the total thickness to be twice of that measured from one face. Therefore, a minimum thickness of approx. $6 \mu\text{m}$ could be detected by HSI. Thus, HSI can be used for an early identification of glass corrosion and intermittent monitoring and documentation of glass objects to prevent loss of historically important yet fragile artefacts. The assessment of the efficiency of cleaning treatments on glass objects can also be a possible field of application.

Supplementary Information The online version contains supplementary material available at <https://doi.org/10.1140/epjp/s13360-024-05009-1>.

Acknowledgements The authors express their gratitude to the colleagues at Swiss National Museum and Norwegian University of Science and Technology, Gjøvik, Norway, especially Markus Sebastian Bakken Storeide (Transmittance Spectroscopy measurements) for their help and support. In addition to this, we would like to thank Dr. Friedrich Menges, Oberstdorf, Germany, for providing free licence of his software Spectragryph.

Funding Open access funding provided by University of Neuchâtel. This research was carried out as part of the CHANGE (change-itn.eu) ITN project funded by the European Union's Horizon 2020 research and innovation programme under the Marie Skłodowska-Curie grant agreement No. 813789.

Data Availability Statement This manuscript has associated data in a data repository. [Authors' comment: The manuscript has data included as electronic supplementary material. The datasets analysed during this study are owned by Swiss National Museum. Data are available from the authors upon reasonable request and permission of Swiss National Museum.]

Declarations

Conflict of interest There are no conflicts of interest concerned with this article and there were no experiments conducted using subjects of any kind.

Open Access This article is licensed under a Creative Commons Attribution 4.0 International License, which permits use, sharing, adaptation, distribution and reproduction in any medium or format, as long as you give appropriate credit to the original author(s) and the source, provide a link to the Creative Commons licence, and indicate if changes were made. The images or other third party material in this article are included in the article's Creative Commons licence, unless indicated otherwise in a credit line to the material. If material is not included in the article's Creative Commons licence and your intended use is not permitted by statutory regulation or exceeds the permitted use, you will need to obtain permission directly from the copyright holder. To view a copy of this licence, visit <http://creativecommons.org/licenses/by/4.0/>.

References

1. A. Schwarz, "kranke" gläser Formaldehydemission und glaskorrosion Untersuchungen am beispiel der glassammlung des schweizerischen landesmuseums. *Zeitschrift Für Schweizerische Archäologie Und Kunstgeschichte* **59**, 371–384 (2002)

2. M. Odlyha, C.J. Bergsten, D. Thickett, Volatile organic compounds (vocs) released by wood, in *Basic Environmental Mechanisms Affecting Cultural Heritage. Under- Standing Deterioration Mechanisms for Conservation Purposes. COST Action D.* ed. by D. Camuffo, V. Fassina, J. Havermans (Nardini, Florence, 2010), pp.107–133
3. A. Schieweck, W. Delius, N. Siwinski, W. Vogtenrath, C. Genning, T. Salthammer, Occurrence of organic and inorganic biocides in the museum environment. *Atmos. Environ.* **41**(15), 3266–3275 (2007)
4. E. Greiner-Wronowa, Influence of organic pollutants on deterioration of antique glass structure. *Acta Phys. Pol. A* **120**(4), 803–811 (2011)
5. G. Verhaar, M.R. Van Bommel, N.H. Tennent, Weeping glass: The identification of species on the surface of vessel glass using ion chromatography. (2016). <https://www.researchgate.net/publication/329268597>
6. L. Robinet, The role of organic pollutants in the alteration of his-toric soda silicate glass. PhD thesis, Université Paris VI, France and University of Edinburgh, Scotland (2006)
7. L. Robinet, C. Hall, K. Eremin, S. Fearn, J. Tate, Alteration of soda silicate glasses by organic pollutants in museums: mechanisms and kinetics. *J. Non-Cryst. Solids* **355**(28–30), 1479–1488 (2009)
8. A. Schwarz, Aspekte zu Ursachen und Behandlungsmöglichkeiten der Hohlglaskorrosion: Dargestellt am Beispiel der Glassammlung des Schweizerischen Landesmuseums Zürich; Diplomarbeit. Doctoral dissertation, Staatliche Akademie der Bildenden Künste (2000)
9. D. Sharma, U. Rothenhaeusler, K. Schmidt-Ott, M. Nurit, Y.C. Carta-gena, G. Le-Goic, E. Joseph, S. George, T. Lombardo et al., in *Monitoring and understanding voc induced glass corrosion using multi- modal imaging techniques*, ed. by R. Furferi. The Future of Heritage Science and Technologies in LNME, Florence: Italy (2023)
10. D. Sharma, U. Rothenhaeusler, K. Schmidt-Ott, E. Joseph, S. George, T. Lombardo, in *Multi-modal Analysis of Transparent Glass to Detect Early Signs of Volatile Organic Compounds-Induced Corrosion due to Contaminated Silica Gel*, eds. by H. Roemich, L. Fair. Recent Advances in Glass and Ceramics Conservation 2022: the 6th Interim Meeting of the ICOM-CC Glass and Ceramics Working Group, Lisbon: Portugal (2022)
11. B.C. Bunker, Molecular mechanisms for corrosion of silica and silicate glasses. *J. Non-Crystalline Solids* **179**, 300–308 (1994)
12. F. Alloteau, P. Lehuédé, O. Majérus, I. Biron, A. Dervanian, T. Charpentier, D. Caurant, New insight into atmospheric alteration of alkali-lime silicate glasses. *Corros. Sci.* **122**, 12–25 (2017)
13. L. Gentaz, T. Lombardo, A. Chabas, C. Loisel, D. Neff, A. Verney-Carron, Role of secondary phases in the scaling of stained-glass windows exposed to rain. *Corros. Sci.* **109**, 206–216 (2016)
14. M.S. Rice, E.A. Cloutis, J.F. Bell III., D.L. Bish, B.H. Horgan, S.A. Mertzman, M.A. Craig, R.W. Renaut, B. Gautason, B. Mountain, Reflectance spectra diversity of silica-rich materials: sensitivity to environment and implications for detections on mars. *Icarus* **223**(1), 499–533 (2013)
15. S. Zaleski, E. Montagnino, L. Brostoff, I. Muller, A. Buechele, C.F.F. Lynn Ward-Bamford, M. Loew, Application of fiber optic reflectance spectroscopy for the detection of historical glass deterioration. *J. Am. Ceram. Soc.* **103**(1), 158–166 (2020)
16. L.B. Brostoff, C.L. Ward-Bamford, S. Zaleski, T. Villafana, A.C. Buechele, I.S. Muller, F. France, M. Loew, Glass at risk: a new approach for the study of 19th century vessel glass. *J. Cult. Herit.* **54**, 155–166 (2022)
17. J.Y. Hardeberg, *Acquisition and Reproduction of Color Images: Colori- metric and Multispectral Approaches* (Universal-Publishers, Parkland, 2001)
18. C. Fischer, I. Kakoulli, Multispectral and hyperspectral imaging tech- nologies in conservation: current research and potential applications. *Stud. Conserv.* **51**(sup1), 3–16 (2006)
19. A.F. Goetz, Measuring the earth from above: 30 years (and counting) of hyperspectral imaging. *Photon. Spectra* **45**(6), 42–47 (2011)
20. B. Park, Future trends in hyperspectral imaging. *NIR News* **27**(1), 35–38 (2016)
21. S. George, J.Y. Hardeberg, J. Linhares, Macdonald, C. Montagner, S. Nascimento, M. Picollo, R. Pillay, T. Vitorino, E. KeatsWebb, A study of spectral imaging acquisition and processing for cultural her- itage. *Digit. Tech. Doc. Preserv. Cultural Herit.* **65**, 206–216 (2018)
22. T. Palomar, C. Grazia, I.P. Cardoso, M. Vilarigues, C. Miliani, A. Romani, Analysis of chromophores in stained-glass windows using visible hyperspectral imaging in-situ. *Spectrochim. Acta Part A Mol. Biomol. Spectrosc.* **223**(11737), 1–9 (2019)
23. E. Rebollo, F. Ratti, G. Cortelazzo, L. Poletto, R. Bertoncetto, New trends in imaging spectroscopy: the non-invasive study of the scrovegni chapel stained glass windows. *O3A Opt. Arts Archit. Archaeol.* **III**(808), 47–56 (2011)
24. A. Babini, S. George, J.Y. Hardeberg, Hyperspectral imaging work-flow for the acquisition and analysis of stained-glass panels. In: *Opticsfor Arts, Architecture, and Archaeology VIII, Proceedings Spie*, vol. 11784, pp. 198–207 (2021)
25. A. Babini, S. George, T. Lombardo, J.Y. Hardeberg, A Portable Set up for Hyperspectral Imaging of Stained-Glass Panels. In: *International Conference Florence Heri-Tech: the Future of Heritage Science and Technologies*, (Springer International Publishing, Cham, 2022) pp. 57–70
26. V.M. Papadakis, B. Müller, M. Hagenbeek, J. Sinke, R.M. Groves, Monitoring chemical degradation of thermally cycled glass-fibre composites using hyperspectral imaging. *Non-Destruct. Charact. Monit. Adv. Mater. Aerosp. Civ. Infrastruct.* **2016**(9804), 201–208 (2016)
27. H.J. Gwang, <https://patents.google.com/patent/WO2016043397A1/en> (2016)
28. W.A. Museum, <https://manual.museum.wa.gov.au/conservation-and-care-collections-2017/glass/preventive-conservation> (2022)
29. J. Schindelin, I. Arganda-Carreras, E. Frise, V. Kaynig, M. Longair, T. Pietzsch, S. Preibisch, C. Rueden, S. Saalfeld, B. Schmid, J.Y. Tinevez, D.J. White, V. Hartenstein, K. Eliceiri, P. Tomancak, A. Cardona, Fiji: an open-source platform for biological-image analysis. *Nat. Methods* **9**(7), 676–682 (2012)
30. F. Menges, Spectragryph-optical spectroscopy software. Tech-nical report, Version 1.2.15, 2016–2020. <http://www.ffmpeg2.de/spectragryph/>
31. A. Pisello, S. De Angelis, M. Ferrari, M. Porreca, F.P. Vetere, H. Behrens, M.C. De Sanctis, D. Perugini, Visible and near-infrared (vnir) reflectance of silicate glasses: characterization of a featureless spectrum and implications for planetary geology. *Icarus* **374**, 114801 (2022)